Compact InGaAsP/InP Asymmetric Mach–Zehnder Coupled Square Ring Modulator

Shuang Wang, Le Wang, Liya Zhao, Bing Qi, and Ke Liu, *Member, IEEE*

***Abstract*— We propose a compact InGaAsP/InP electro-optic ring modulator operated with coupling modulation that can circumvent the bandwidth limitation and large minimum bend radius of a ring. This device consists of frustrated total internal reflection (TIR) couplers and TIR mirrors serving as 90° waveguide bends, forming the configuration of an asymmetric rectangular Mach–Zehnder interferometer coupled to a square ring resonator (SRR). A discrete-time dynamic model and finite-difference time-domain method are used to evaluate the device performances, and the theoretical results show an operating frequency up to 60 GHz, the maximum extinction ratio of ∼12 dB, the low electrical energy of ∼60 fJ/bit, and a compact chip size of ∼18 μm × 29 μm, respectively. The enabling component of the SRR represents >100-fold footprint reduction on a chip. This compact device can be potentially applied in large-scale InP-based photonic integrated circuits.**

***Index Terms*— Integrated photonics, electro-optic modulators, Mach-Zehnder interferometer, ring resonator, trench coupler.**

I. Introduction

MICRORING resonator modulators have gained significant scientific and technological attention in recent years due to their compact sizes and low power consumption [1], [2]. A typical microring modulator consists of a single circular ring coupled to an input/output bus waveguide [3], having a modulation section within the ring resonator which changes the refractive index and/or loss inside the cavity. This conventional mechanism is known as intracavity index/loss modulation, which is fundamentally bounded by cavity photon lifetime, resulting in the modulation rate inherently limited by its cavity linewidth (i.e., inversely proportional to quality (Q) factor) [4].

Recently a coupling modulation scheme was proposed to circumvent the bandwidth limitation [5], where the coupling strength between the microring and the input/output bus waveguide is modulated rather than the intracavity index or loss. To date most of coupling modulation modulators were demonstrated either on a Silicon-on-insulator (SOI) platform [4]–[6] or on an InP substrate [7] through the configurations of a microring interacting with Mach-Zehnder interferometer (MZI) couplers. However, the relatively lower index contrast of an InGaAsP/InP platform, as compared to SOI does lead to a larger radius of ring resonator, and the advised minimum bend radius is up to 500 μm for a shallow etched ridge waveguide [8].

Here we propose an InGaAsP/InP asymmetric MZI coupled square ring electro-optic (EO) modulator. This novel modulator consists of two trench couplers and four 90° waveguide bends, exhibiting a rectangular layout configuration. We theoretically investigate the modulator design parameters and performances by using a discrete-time dynamic model and a finite difference time domain (FDTD) numerical method, respectively. Note, the square ring resonator (SRR) shown here can significantly reduce the device footprint, and avoid the limitation by radius of curvature for a circular ring counterpart due to its large bending loss, while make the cavity length shorter and the free spectral range (FSR) larger, and thus increase the device's modulation bandwidth.

II. Modulator Configuration

The InGaAsP/InP EO modulator comprises an asymmetric MZI coupled to a SRR (Fig. 1a), and both structures share one section of a straight waveguide. A single "slash" deep narrow trench that is aligned 45° with respect to the light propagation direction is created at the intersection of two waveguides, forming a trench-coupler serving as a light splitter or combiner (Fig. 1b). The trench-coupler is operated with a principle of frustrated total internal reflection (TIR) [9]. Note, if the trench width is comparable to the penetration distance of the evanescent wave, light can tunnel for transmission in addition to reflection. The other key components are the TIR mirrors, which are located at the "U" shape waveguide corners with 45° to the light propagation direction, and thus act as the 90° waveguide bends. Towards applying a driving voltage, V_B, a P-metal contact is atop the inverted "U" shape waveguide phase shift arm in the MZI, and an N-metal contact can be deposited on the backside of the device.

To demonstrate the feasibility of processing a narrow trench etching, the epitaxial multi-quantum well layers were first grown on an InP substrate forming a top-down P-I-N structure. A vertical and deep trench with an opening of ∼300 nm was fabricated using HBr-based chemistry by an

Manuscript received April 5, 2017; revised June 18, 2017; accepted June 27, 2017. Date of publication June 30, 2017; date of current version July 19, 2017. This work was supported in part by the National Natural Science Foundation of China under Grant 61377059, in part by the Beijing Natural Science Foundation under Grant 4142004, and in part by the Development Foundation for Optoelectronics Technology Laboratory, Ministry of Education, under Grant PXM2017_014204_500034. *(Corresponding author: Ke Liu.)*

S. Wang, L. Wang, and L. Zhao are with the Key Laboratory of Optoelectronics Technology, Ministry of Education, Faculty of Information Technology, Beijing University of Technology, Beijing 100124, China (e-mail: czyfws@163.com; 972049319@qq.com; 1558217864@qq.com).

B. Qi is with the Department of Computer Science, Methodist University, Fayetteville, NC 28311 USA (e-mail: bqi@methodist.edu).

K. Liu is with the Key Laboratory of Optoelectronics Technology, Ministry of Education, Faculty of Information Technology, Beijing University of Technology, Beijing 100124, China, and also with the Department of Electrical and Computer Engineering, George Washington University, Washington, DC 20052 USA (e-mail: liuke@bjut.edu.cn).

Color versions of one or more of the figures in this letter are available online at http://ieeexplore.ieee.org.

Digital Object Identifier 10.1109/LPT.2017.2721977

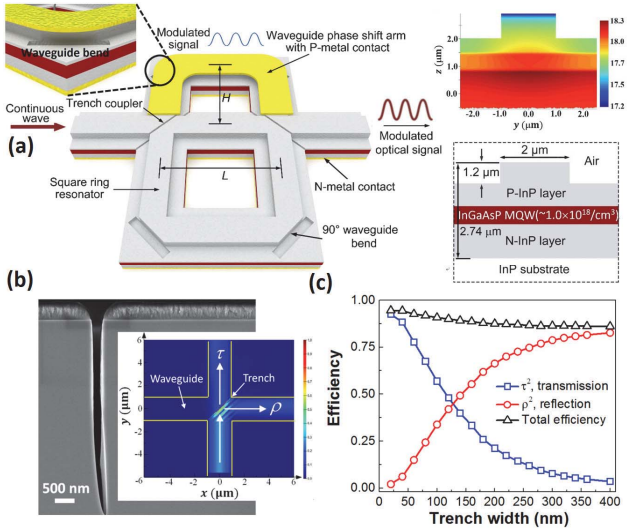

Fig. 1. (a) Perspective view of an InGaAsP/InP asymmetric MZI coupled SRR EO modulator, where L is the side length of the SRR, and H is the longitudinal length of the asymmetric MZI. The top-left inset shows the existence of a waveguide bend at the corner under the P-metal contact. The top-right inset gives a carrier concentration profile at the waveguide cross-section with V_B =1.8 V, and the bottom-right inset shows a single-mode ridge waveguide geometry of phase shift arm at 1550 nm wavelength, with the carrier concentration of $\sim 1.0 \times 10^{18}/\text{cm}^3$ at the MQW region for $\Delta n_{eff} = \sim 0.01$. (b) Cross-sectional scanning electron microscopy image of a trench with a high aspect ratio of >14:1 etched on an InGaAsP/InP wafer (Fabrication conditions: 10 sccm HBr, 2 mTorr pressure, 800 W ICP and 240 W platen powers, 160°C, and 6 min etching time). The inset shows the light power distribution profiles within a 3 dB trench-coupler, where τ (ρ) is the transmission (reflection) coupling coefficient. (c) Efficiency of a trench-coupler filled with alumina as a function of trench widths for various τ and ρ, and $\rho^2 + \tau^2$ (total efficiency), respectively.

Oxford PlasmaLab 100 inductively coupled plasma (ICP) tool [10], showing a high aspect ratio of >14:1(Fig. 1b). The waveguide bends can be realized by etching a broad trench with an opening of >1.0 μm, having the similar processing conditions for the narrow trench fabrication. The trench width required for a fixed ratio of light power splitting is related to the index of dielectric material filled in the trench. We characterized the splitting ratio and total efficiency as a function of trench width by using Lumerical FDTD Solutions (Fig. 1c). An about 130 nm wide trench filled with alumina (refractive index, n ~1.75 at 1550 nm wavelength) forms a 3-dB coupler for transverse-electric (TE) light polarization. An averaged total efficiency of ~90% is attained for this coupler.

The rectangular and square layout configurations for MZI and ring resonator can be built by utilizing the trench-coupler and TIR mirrors, which easily scale its pattern in the two-dimensional directions, avoiding the excess longer stack in one dimension of the device. Similar rectangular resonator design without a tunable coupler was reported using TIR mirrors for an intensity modulator [11]. Here we show the footprint of the SRR can be reduced by at least 100 fold in contrast to a typical InGaAsP/InP ring with 100 μm radius [12]. Examples of trench couplers-based devices have been successfully demonstrated for Silicon MZI thermo-optic switch [13], InP-based PIC filter [10] and flattened ring laser [14].

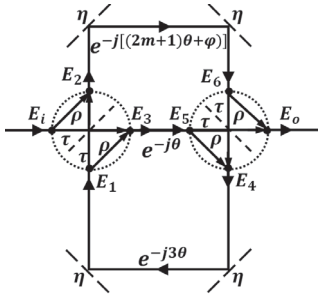

Fig. 2. Signal flow diagrams of the asymmetric MZI coupled SRR modulator. The dashed circles and slashes represent trench couplers and 90° waveguide bends, respectively, where m is the ratio between H and L, i.e., $H = mL$, θ is the phase change for light passing through a L-length waveguide, φ is the extra phase shift in the "U" shape waveguide arm due to an external V_B applied, and η is the reflection efficiency of 90° waveguide bend. $E_1 \sim E_6$ are the internal electric field amplitudes of output (input) light from (to) the trench couplers, respectively. $E_i(E_o)$ is the external electric field amplitude at the input (output) ports, respectively.

For coupling modulation, the parameters such as phase and loss in the intracavity (i.e., SRR) remain constant, while the through- and cross-coupling strength is modulated. The coupling strength between the MZI and SRR can be electro-optically controlled by the waveguide phase-shift arm through the index change resulting from carrier-induced effect on InGaAsP/InP materials with a proper V_B applied.

III. Discrete-Time Dynamic Model

For a ring resonator based device, it requires some time to generate the steady-state electric field distribution of light. Especially for a high-frequency case, delay time is a key factor that can significantly influence the modulation bandwidth. Therefore, steady-state analysis via coupled mode theory is not able to predict dynamic performance. Here we develop a discrete-time dynamic model to simulate optical field distribution through an iterative computation method [6].

Based on the signal flow diagrams (Fig. 2), the transfer matrix of the left trench-coupler close to the input port can be expressed by,

$$\begin{bmatrix} E_2(t) \\ E_3(t) \end{bmatrix} = \begin{bmatrix} -j\rho & \tau \\ \tau & -j\rho \end{bmatrix} \begin{bmatrix} E_i(t) \\ E_1(t) \end{bmatrix} \tag{1}$$

where t is the discrete-time variable. Signal passing through a waveguide can generate time and phase delay. The time delay Δt is set for light after a L-length waveguide. The internal electric field amplitudes, i.e., E_5 and E_6, to the right trench-coupler is written by,

$$E_5(t) = 10^{-\alpha L/20} E_3(t - \Delta t)\, e^{-j\theta} \tag{2}$$

$$E_6(t) = 10^{-(2m+1)\alpha L/20} \eta^2 E_2[t - (2m+1)\Delta t] e^{-j[(2m+1)\theta+\varphi]} \tag{3}$$

where α is the waveguide loss coefficient per unit length in decibels, and α = 2 dB/cm is used here[15]. Towards achieving η, a FDTD simulation method is utilized. A fundamental TE mode source is excited at the input waveguide of a TIR mirror, and the reflected (input) power recorded by the power monitors are used to calculate the efficiency.

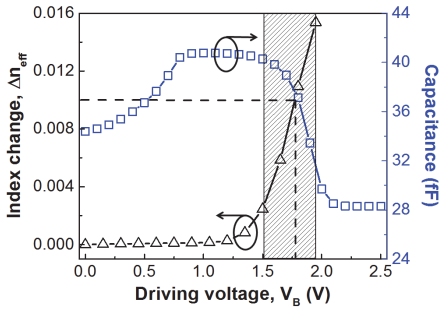

Fig. 3. Simulated effective index change and capacitance dependency on V_B applied for the InGaAsP/InP asymmetric MZI coupled SRR modulator at a TE polarization state. The dashed line shows that $\Delta n_{eff} =\sim 0.01$ at $V_B =\sim 1.8$ V. The corresponding device capacitance is ~37 fF, where the P-metal contact width of 5.0 μm and the length of ~35 μm are used for the analysis.

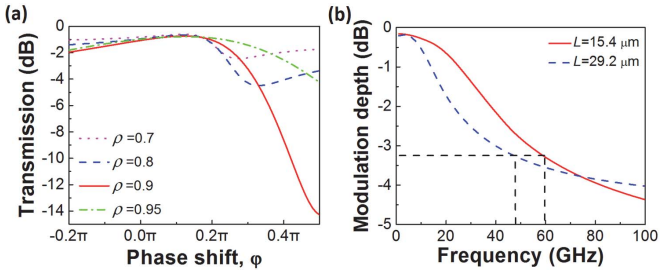

Fig. 4. (a) Transmission characteristic of the modulator dependency on the coupler reflection coefficient at $\lambda_m = 1.551$ μm wavelength. $L = 15.4$ μm is used here. (b) Modulation depth as a function of frequency at the two side lengths of square ring modulators. Here MD in dB is defined by $10\log_{10}(P_{max} - P_{min})/(P_{max} + P_{min})$, where P_{max} (P_{min}) is the maximum (minimum) output power at the modulator output. $\rho = 0.9$ and $\tau = 0.37$ are used here.

We find an optimizing value of $\eta = 96\%$. The phase change, $\theta = 2\pi n_{eff} L/\lambda$, n_{eff} is the mode effective refractive index, and $n_{eff} = 3.184$ is calculated for the TE fundamental mode via a FIMMWAVE mode solver, λ is the light wavelength in vacuum. Similarly, the transfer matrix of the right trench-coupler close to the output port can be expressed by,

$$\begin{bmatrix} E_o(t) \\ E_4(t) \end{bmatrix} = \begin{bmatrix} -j\rho & \tau \\ \tau & -j\rho \end{bmatrix} \begin{bmatrix} E_6(t) \\ E_5(t) \end{bmatrix} \quad (4)$$

$$E_1(t) = 10^{-3\alpha L/20} \eta^2 E_4(t - 3\Delta t)\, e^{-j3\theta} \quad (5)$$

Solving (1) ~ (5), we have the iteration starting at $t = 0$, since the amplitudes of $E_1 \sim E_6$ are zero due to without optical field distribution inside the device at $t < 0$. While at any time of $t > 0$, various device performance can be evaluated in terms of the transmission characteristics.

IV. Modulator Design

This design is divided into three steps; (i) determine m and L for a π phase shift at an expected modulation wavelength, λ_m, (ii) find V_B for an extra phase shift, φ, and (iii) optimize the splitting ratio of the trench-coupler used for the modulator.

Regarding (i), the analysis from the discrete-time dynamic model shows that m and L both influence the modulated wavelength, e.g., $\lambda_m = 1.575$ μm for $H = L$, and $\lambda_m = 1.515$ μm for $H = 0.5L$. $m = 0.75$ is thus determined for the target of $\lambda_m = 1.55$ μm. The optical path length difference equation can thus give $L = 15.4$ μm for a π phase shift at the inverted "U" shape waveguide arm without V_B applied. This leads to destructive interference and zero coupling into the SRR for an ON state. For the case (ii), the relationship between Δn_{eff} and V_B can be achieved through a P-I-N junction model via Lumerical DEVICE software (Fig. 3), where a drift-diffusion transport solver is used to analyze the electrical characteristics by defining the waveguide geometry (Fig. 1a bottom-right inset) and doping profile (Fig. 1a top-right inset), and to simulate the charge distribution in the waveguide dependent on a voltage. φ can be related to the applied voltage, V_B(t), by $\varphi = 2\pi L_c/\lambda_m \cdot [\Delta n_{eff}(V_B)]$, where L_c is the P-metal contact length, i.e., $L_c = (2m + 1)L$, $\Delta n_{eff}(V_B) = -0.042 + 0.029 \cdot V_m(t)$ is linearly fitted in the shaded region (Fig. 3), and V_m(t) is the modulation signal, which is described as $V_m(t) = V_0 + k \cdot \sin(2\pi f t)$ for the sinusoidal modulation, where V_0 is the bias voltage, k is the sinusoidal signal amplitude, and f is the frequency. The EO index change results in an extra phase shift that enables coupling into the ring with an OFF state.

Moving on to the case (iii), we find that the more reflected power than the transmitted (i.e., $\rho > \tau$) for the trench-coupler is beneficial to this modulator due to the sufficiently high Q-factor obtained for the SRR. A tolerance analysis of trench splitting ratios was performed based on the phase shift required for the modulation (Fig. 4a). $\varphi = 0.2\ \pi$, and $0.5\ \pi$ are optimized for the $L = 15.4$ μm SRR modulator at the coupler coefficients of $\rho = 0.9$ and $\tau = 0.37$. Compared to typical MZI-based optical modulators, the current design can attain light modulation through a small change of φ.

High speed optical modulators are desired in PICs. We compared the modulation bandwidth of the modulators with different L (Fig. 4b). Here both the optical dynamics of the SRR and electrical response of the modulation section are included, without considering the effect of carrier drifting time. The bandwidth is defined as the frequency at which the modulation depth (MD) decays to the point of -3 dB. The frequency of 60 (48) GHz is evaluated for the $L = 15.4$ (29.2) μm SRR modulator, respectively. The small L results in a short length of the resonant cavity, therefore leading to a larger FSR. Further reduced L can lead to a smaller λ_m. The minimal linewidth of the resonator is simulated to be ~0.36 nm, which corresponds to a frequency bandwidth of ~45 GHz. If the modulation frequency is larger than the linewidth, the coupling modulation is usually more efficient than modulating the resonance wavelength.

V. FDTD Analysis and Discussion

A FDTD numerical method is adopted to further validate the modulation function (Fig. 5). Here only the index modulation is considered, and the impact of material chirp (i.e., loss modulation) is neglected. The trench opening of ~280 nm is set, which corresponds to the coupler coefficients of $\rho = 0.89$ and $\tau = 0.32$ (Fig. 1c).

We can observe the light modulation in the transmission spectra comparing the cases with and without V_B applied,

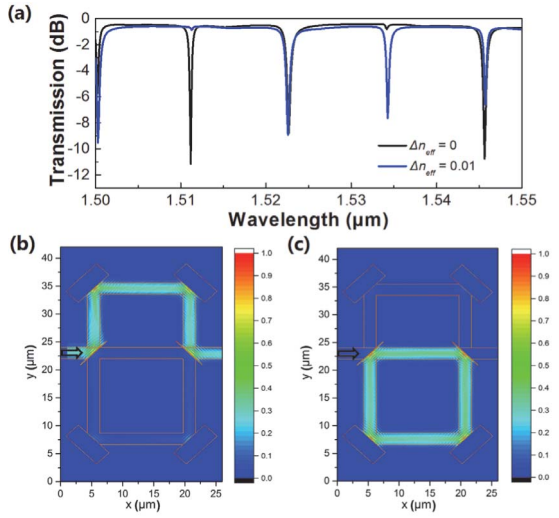

Fig. 5. (a) Transmission spectra of the InGaAsP/InP asymmetric MZI coupled SRR modulator having $L = 15.4$ μm without and with a V_B by a FDTD method. The light intensity distribution profiles at (b) $V_B = 0$, $\Delta n_{eff} = 0$, and (c)$V_B = 1.8$ V, $\Delta n_{eff} = 0.01$ at $\lambda_{m1} = 1.511$ μm, respectively. The arrow indicates light incident direction to the device.

at the resonance of $\lambda_{m1} = 1.511$ μm and $\lambda_{m2} = 1.534$ μm, respectively (Fig. 5a). Other resonant wavelengths are not effectively modulated (e.g., 1.522 μm) due to the necessary resonance selection of the SRR through the MZI coupler. The maximum extinction ratio (ER) of ∼12 dB is obtained at $\lambda_{m1} = 1.511$ μm, which also relates to a Q-factor of ∼4100 for the SRR. Note, a single arm modulation of the MZI coupler can lead to both modulation of the resonant wavelength and coupling strength [16]. Fig. 5(a) only shows the case of the coupling strength tuning at a fixed resonance. In practice, independent tuning of the coupling strength can be achieved by using thermal tuners in the MZI-coupler arms [4], which can be adjusted to create a common or differential phase-shift. The coupling modulation is verified through the light intensity distribution profiles with and without V_B (Fig. 5b and c). Without V_B applied, light is clearly transmitted through the longer waveguide phase-shift arm in the MZI, for the ON state. While with $V_B = 1.8$ V, light is completely coupled to the SRR, for the OFF state. The total insertion loss of the modulator is estimated to be ∼1.8 dB for the ON state by monitoring the output power.

Energy per bit is one of the key performances representing the power efficiency. The electrical energy consumption is estimated by $E_m = 1/2 \cdot (CV_B^2)$ [2], [17], where C is the device capacitance. The capacitance of the metal-contact covered regions depending on V_B is evaluated by using a small-signal analysis method in Silvaco software (Fig. 3). A capacitance of ∼37 fF is attained at $V_B =\sim 1.8$ V. The theoretical electrical energy of ∼60 fJ/bit is thus calculated for this modulator, which potentially meets the power efficiency target (i.e., <0.1 pJ/bit) at a distance of $1 \sim 5$ cm for chip-to-chip communications [18].

VI. Conclusions

We have designed and numerically investigated an InGaAsP/InP asymmetric MZI coupled SRR EO modulator based on a coupling modulation mechanism. This novel modulator incorporates two frustrated-TIR trench couplers and four TIR mirrors, forming the configuration of a rectangular MZI and a SRR, which can be flexibly extended at the two-dimensional scales due to the feature of light transmitted and reflected at the 90° directions. The theoretical results show an operating frequency up to 60 GHz, the maximum ER of ∼12 dB at a resonant wavelength of 1.511 μm, the low electrical energy of ∼60 fJ/bit, and a compact chip size of ∼18 μm × 29 μm. The enabling component of the SRR represents a >100-fold footprint reduction on a chip. This compact device configuration can be applied in large-scale InP-based PICs such as high density on-chip optical interconnects, and potentially allow for a cheaper cost per square millimeter of wafers.

References

[1] G. T. Reed, G. Mashanovich, F. Y. Gardes, and D. J. Thomson, "Silicon optical modulators," *Nature Photon.*, vol. 4, pp. 518–526, Jul. 2010.
[2] K. Liu, C. R. Ye, S. Khan, and V. J. Sorger, "Review and perspective on ultrafast wavelength-size electro-optic modulators," *Laser Photon. Rev.*, vol. 9, no. 2, pp. 172–194, Mar. 2015.
[3] Q. Xu, B. Shmidt, S. Pradhan, and M. Lipson, "Micrometre-scale silicon electro-optic modulator," *Nature*, vol. 435, no. 7040, pp. 325–327, May 2005.
[4] W. D. Sacher *et al.*, "Coupling modulation of microrings at rates beyond the linewidth limit," *Opt. Exp.*, vol. 21, no. 8, pp. 9722–9733, 2013.
[5] W. D. Sacher and J. K. S. Poon, "Characteristics of microring resonators with waveguide-resonator coupling modulation," *J. Lightw. Technol.*, vol. 27, no. 17, pp. 3800–3811, Apr. 2009.
[6] J. Hong and Y. Enami, "Modeling and analysis of microring resonator modulators with feedback waveguide coupling," *J. Lightw. Technol.*, vol. 29, no. 21, pp. 3243–3249, Dec. 2011.
[7] W. M. J. Green, R. K. Lee, G. A. DeRose, A. Scherer, and A. Yariv, "Hybrid InGaAsP-InP Mach–Zehnder racetrack resonator for thermooptic switching and coupling control," *Opt. Exp.*, vol. 13, no. 5, pp. 1651–1659, Mar. 2005.
[8] M. Smit *et al.*, "An introduction to InP-based generic integration technology," *Semicond. Sci. Technol.*, vol. 29, no. 8, Jun. 2014, Art. no. 083001.
[9] N. R. Huntoon, M. P. Christensen, D. L. MacFarlane, G. A. Evans, and C. S. Yeh, "Integrated photonic coupler based on frustrated total internal reflection," *Appl. Opt.*, vol. 47, no. 30, pp. 5682–5690, Oct. 2008.
[10] D. L. MacFarlane *et al.*, "Experiment and theory of an active optical filter," *IEEE J. Quantum Electron.*, vol. 48, no. 3, pp. 307–317, Mar. 2012.
[11] Y. Zhang, B. Pile, and G. W. Taylor, "Design of micro resonator quantum well intensity modulator," *Opt. Quantum Electron.*, vol. 44, no. 14, pp. 635–648, Apr. 2012.
[12] D. G. Rabus, Z. Bian, and A. Shakouri, "A GaInAsP-InP double-ring resonator coupled laser," *IEEE Photon. Technol. Lett.*, vol. 17, no. 9, pp. 1770–1772, Sep. 2005.
[13] K. Liu, C. Zhang, S. Mu, S. Wang, and V. J. Sorger, "Two-dimensional design and analysis of trench-coupler based silicon Mach–Zehnder thermo-optic switch," *Opt. Exp.*, vol. 24, no. 14, pp. 15845–15853, Jul. 2016.
[14] J. S. Parker, E. J. Norberg, Y. J. Hung, B. Kim, R. S. Guzzon, and L. A. Coldren, "InP/InGaAsP flattened ring lasers with low-loss etched beam splitters," *IEEE Photon. Technol. Lett.*, vol. 23, no. 9, pp. 573–575, May 2011.
[15] P. Verboom *et al.*, "A long InGaAsP/InP waveguide section with small dimensions," *IEEE Photon. Technol. Lett.*, vol. 4, no. 10, pp. 1112–1114, Oct. 1992.
[16] C. Li, L. J. Zhou, and A. W. Poon, "Silicon microring carrier-injection-based modulators/switches with tunable extinction ratios and OR-logic switching by using waveguide cross-coupling," *Opt. Exp.*, vol. 15, no. 8, pp. 5069–5076, Apr. 2007.
[17] D. A. B. Miller, "Energy consumption in optical modulators for interconnects," *Opt. Exp.*, vol. 20, no. S2, pp. A293–A308, Mar. 2012.
[18] E. Agrell *et al.*, "Roadmap of optical communications," *J. Opt.*, vol. 18, no. 6, May 2016, Art. no. 063002.